Available online at www.sciencedirect.com
ScienceDirect
Journal of Power Sources 163 (2006) 339–348
JOURNAL OF POWER SOURCES
www.elsevier.com/locate/jpowsour

Water-stable crosslinked sulfonated polyimide–silica nanocomposite containing interpenetrating polymer network

Chang Hyun Lee [a], Shin Young Hwang [a], Joon Yong Sohn [a], Ho Bum Park [a], Ju Young Kim [b], Young Moo Lee [a,*]

[a] *School of Chemical Engineering, College of Engineering, Hanyang University, Seoul 133-791, Republic of Korea*
[b] *Department of Advanced Materials Engineering, Kangwon National University, Samcheok, Kangwon 245-711, Republic of Korea*

Received 18 July 2006; received in revised form 17 August 2006; accepted 15 September 2006
Available online 27 October 2006

Abstract

Sulfonated polyimide (SPI) interpenetrating polymer network (IPN) (IXSPI)–silica (SiO_2) nanocomposite membranes were fabricated as proton conducting solid electrolytes for fuel cells. Urethane acrylate non-ionomers (UANs) were used as dispersants to homogeneously distribute nano-sized SiO_2 and, simultaneously, as crosslinkers to induce IPN structure formation. IXSPI–SiO_2 nanocomposite membranes showed high proton conductivity and hydrolytic stability, and low methanol permeability as compared with those of pristine SPI. Interestingly, the casting solvent for membrane fabrication influenced membrane performances, especially proton conductivity. In particular, dimethyl sulfoxide exhibited a strong interaction with sulfonic acid groups in the polymer matrix, which hindered them from spontaneously releasing protons and reduced the proton conductivity and electrochemical performances of the resulting membranes. Crosslinkers with long polyethylene oxide chains also contributed to improved proton conductivity and increased single cell performances.

Keywords: Sulfonated polyimide–silica nanocomposite; Membrane; Urethane acrylate nonionomer; Solvent effect; Crosslinker size

1. Introduction

Organic–inorganic composites have recently received much attention in biomaterials [1], wave guides [2], nonlinear optical substrate [3,4], and as electrolytes in secondary battery [5] and fuel cell [6] applications because the composites combine unique properties. These include high processability and excellent mechanical properties derived from organic polymers and inorganic particles, respectively. Among their numerous applications, proton conductive composites, in particular, have been highlighted as one potential proton exchange membrane (PEM). The composite type PEMs are expected to replace or modify commercial perfluorinated sulfonic acid (PFSA) membranes including Nafion®.

Trials have been carried out to incorporate inorganic oxides such as silica (SiO_2) [7–9], alumina (Al_2O_3) [9], zirconium oxide (ZrO_2) [9,10] and titanium oxide (TiO_2) [9] into polymer matrices for self-humidification, reduction of electro-osmotic drag and methanol crossover, and for the improvement of mechanical, thermal, and dimensional stability. The most important issues in organic–inorganic composite membranes are a homogeneous distribution of inorganic oxides in the polymer matrix, a fabrication of composites with high reliability in membrane performances, and an establishment of the factors (chemical structure of the polymer matrix, kinds of inorganic fillers [7–9], sources of inorganic fillers [11–17], and casting solvent [18–20]) which affect membrane performances.

In most cases, a sol–gel synthetic route using alkoxide precursors [11–15] has been used to homogeneously distribute inorganic oxide particles *in situ* into a polymer matrix. However, the morphologies and physico-chemical properties of the resulting hybrid membranes were easily affected by many factors including the types of alkoxide precursors used, pH in the

* Corresponding author. Tel.: +82 2 2220 0525; fax: +82 2 2291 5982.
E-mail address: ymlee@hanyang.ac.kr (Y.M. Lee).

0378-7753/$ – see front matter © 2006 Elsevier B.V. All rights reserved.
doi:10.1016/j.jpowsour.2006.09.023

reaction medium, solvents, reaction temperature and pressure, and concentration of reactants. On the other hand, direct mixing of SiO_2 nanoparticles is a simple and convenient approach to fabricate composite membranes where fumed SiO_2 particles should be well distributed at the nanoscale. However, direct mixing in an ultrasonic bath, which is used in most cases [16], shows a limitation of content and an irregular distribution of SiO_2, with aggregation or segregation of SiO_2 particles.

The modified approach to direct mixing is the use of amphiphilic dispersants exhibiting both hydrophilic and hydrophobic properties with nanosized fumed SiO_2. In our previous study [17], the ability of the dispersants to form a nano-dispersed SiO_2 phase within sulfonated polymers and to fabricate organic–inorganic composites with high reproducibility has been reported. Here, dispersants accompanied with SiO_2-induced peculiar microstructures strongly depending upon the polymer matrix. That is, the dispersants induced a formation of IPN and, simultaneously, acted as compatibilizers to lower the immiscibility of monomers with different hydrophilicities. IPN structure was generally used to enhance dimensional stability, mechanical strength, and resistance to degradation of the resulting polymers [21].

The objective of this study was to prepare organic–inorganic nanocomposites in combination with IPN and a crosslinked structure with a lot of merits mentioned above, and to determine the effects of the integrated microstructure on PEM performances. For this, a synthetic surfactant, urethane acrylate non-ionomer (UAN) in Fig. 1, was used as a dispersant as well as an IPN-type crosslinker. The goal of this research was to systematically investigate the effects of the casting solvent and chain length of the hydrophilic segment in UAN on membrane performances. In several studies [18–20], it was reported that *N*,*N*-dimethylformamide (DMF) is a poor solvent which reduces proton conductivity of sulfonated polymers. Other solvents which negatively influence PEM performances were previously unreported. Finally, electrochemical single cell performances using the polymer system are presented here in comparison with those using Nafion® membrane under operation conditions in proton exchange membrane fuel cell (PEMFC) and direct methanol fuel cell (DMFC).

2. Experimental

2.1. Materials

1,4,5,8-Naphthalenic tetracarboxylic dianhydride (NTDA), 3,5-diaminobenzoic acid (DBA), and 4,4′-diaminodiphenyl ether (ODA) for use as monomers to fabricate polymer matrix were purchased from Tokyo Kasei Co. (Tokyo, Japan) and used as received. ODA was converted into 4,4′-diaminodiphenyl ether-2,2′-disulfonic acid (SODA) through sulfonation using concentrated sulfuric acid (95%, Aldrich, WI, USA) and fuming sulfuric acid (SO_3, 30%, Aldrich, WI, USA) [22]. Benzoic acid and triethylamine (Et_3N) were purchased from Aldrich Chemical Co. (WI, USA) and used as a catalyst and liberator of protonated amino groups, respectively. *m*-Cresol, dimethyl sulfoxide (DMSO, 99.9%, ACS reagent), 1-methyl-2-pyrrolidinone (NMP, 99.5%), DMF (99.8%), dimethyl acetamide (DMAc, 99.8%) were used as solvents. Furthermore, poly(propylene oxide triol) (PPO triol, MW = 1000), 2,4-toluene diisocyanate (TDI), 2-hydroxyethyl methacrylate (2-HEMA), 2,2′-azobisiso-butyronitril (AIBN) and polyethylene glycol (PEG, MW = 200, 600, 1000, and 3400) were purchased from Aldrich Chemical Co. (WI, USA) and used to synthesize amphiphilic UAN *via* an established three-step process as previously reported [17,23]. Two types of nanosized fumed SiO_2 such as Aerosil® 200 (hydrophilic SiO_2, BET surface area = $200 \pm 25\ m^2\ g^{-1}$) and Aerosil® 812 (hydrophobic SiO_2, BET surface area = $220 \pm 25\ m^2\ g^{-1}$) with average particle size of 12 and 7 nm were purchased from Degussa Chemical Co. (Dusseldorf, Germany), respectively. Prior to use, SiO_2 particles were dried at 80 °C and 3–5 mmHg.

2.2. Fabrication of pristine SPI and IXSPI–SiO_2 nanocomposite

Pristine SPI as a polymer matrix was fabricated through solution-thermal imidization using SODA (1.6 mmol), DBA (2.4 mmol), and NTDA (4.0 mmol) as reported in our previous publications [24,25]. As a result, a fiber-like precipi-

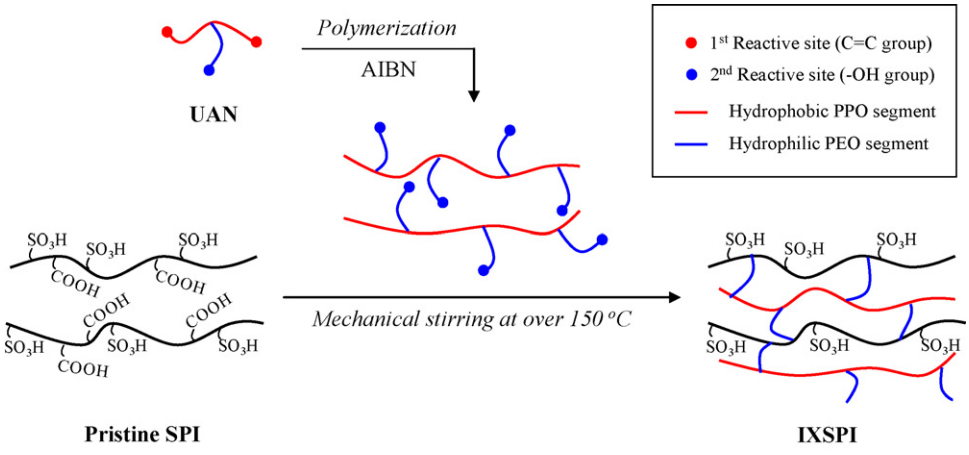

Fig. 1. Schematic diagram of UAN and IXSPI, and formation of IPN structure.

Table 1
Nomenclature of IXSPI–SiO_2 nanocomposites

Sample[a]	UAN			Fumed SiO_2		Solvent
	Molecular weight of PPO (g mol^{-1})	Molecular weight of PEG (g mol^{-1})	Number of PEO units (mol)	Types of SiO_2	SiO_2 content (wt.%)	
Pristine SPI–*d*[b]						DMSO
Pristine SPI–*m*[b]						*m*-Cresol
SPI–0–hl–1–*d*[b]				Aerosil 200 (hydrophilic SiO_2)	1	DMSO
SPI–0–hl–1–*m*[b]					1	*m*-Cresol
SPI–0–hb–1–*d*[b]				Aerosil 812 (hydrophobic SiO_2)	1	DMSO
SPI–0–hb–1–*m*[b]					1	*m*-Cresol
IXSPI–22–hl–0–*d*[b]	1000	1000	22			DMSO
IXSPI–22–hl–0–*m*[b]	1000	1000	22			*m*-Cresol
IXSPI–22–hl–1–*d*[b]	1000	1000	22	Aerosil 200 (hydrophilic SiO_2)	1	DMSO
IXSPI–22–hl–1–*m*[b]	1000	1000	22		1	*m*-Cresol
IXSPI–22–hb–1–*d*[b]	1000	1000	22	Aerosil 812 (hydrophobic SiO_2)	1	DMSO
IXSPI–22–hb–1–*m*[b]	1000	1,000	22		1	*m*-Cresol
IXSPI–4–hl–1–*m*[b]	1000	200	4		1	*m*-Cresol
IXSPI–13–hl–1–*m*[b]	1000	600	13	Aerosil 200 (hydrophilic SiO_2)	1	*m*-Cresol
IXSPI–22–hl–1–*m*[b]	1000	1000	22		1	*m*-Cresol
IXSPI–74–hl–1–*m*[b]	1000	3400	74		1	*m*-Cresol

[a] Types of SPI (SPI or IXSPI)–number of PEO units in UAN–types of SiO_2 (hl or hb)–SiO_2 content–casting solvent. Here, IXSPI means SPI containing UAN.
[b] DMSO (*d*) and *m*-cresol (*m*) were used as casting solvents.

tate of pristine SPI was obtained after pouring into cold acetone, filtration, washing, and drying in a vacuum oven at 120 °C. Then, pristine SPI was re-dissolved in *m*-cresol and DMSO. The pretreated mixture comprising fumed silica particles (1 wt.%) and UAN (MW = 1000 g mol^{-1}) was added to pristine SPI solution. AIBN was used as a radical initiator in each solvent. The mixture was mechanically stirred at over 150 °C for 1 day to obtain a brownish IXSPI–SiO_2 nanocomposite solution. Other IXSPI–SiO_2 nanocomposites were also fabricated with UANs having different hydrophilic chain lengths following the same procedure. SPIs containing only UAN (SPI–22–hl–0) or SiO_2 particles (SPI–0–hl–1 or SPI–0–hb–1) were fabricated for comparison. The nomenclature on each IXSPI–SiO_2 nanocomposite is briefly summarized in Table 1.

Fourier transform infrared (FT-IR) of IXSPI (KBr): 1720, 1680 (C=O), 1407 (C–N–C), 1254 (S=O), 1124, 1730–1735 (–COO–), 1087 (SO_3^-), 918 (S–OH), 744 (O=C–N)

2.3. Membrane formation and acidification

All the resulting membranes were obtained in Et_3N salt form after casting each solution (∼15 wt.%) onto a glass plate, drying at 80 °C for 2 h, and heating at 180 °C for 10 h under vacuum. Each membrane was soaked in methanol under ambient condition for 8 h to remove any residual solvents. After consecutive treatment in deionized water and 1 M hydrochloric acid, the membrane was peeled off from the glass plate and converted into protonated (H^+) form. Then, the protonated membrane was washed with deionized water for 1 day and dried in vacuum oven at 160 °C.

2.4. Polymer and membrane characterization

The FT-IR spectra were measured with a Nicolet Magna IR 760 spectrometer (Madison, WI, USA) in the range of 2000–500 cm^{-1}. The solubility of protonated SPI membranes in common polar aprotic solvents was measured to confirm crosslinked structure based on IPN. The uniform distribution of SiO_2 particles in pristine SPI was evaluated with transmission electron microscopy (TEM, FEI Tecnai G2 20, FEI Company, Hillsboro, OR, USA) as well as field emission scanning electron microscopy (FE-SEM, JEOL Model JSF 6340F, Tokyo, Japan). The sample for TEM measurement was ultra-sectioned using a microtome equipped with a diamond knife and collected using a 200 mesh copper grid. The TEM image was obtained from a Tecnai G2 gun-type apparatus running at an acceleration voltage of 200 kV. The average *d*-spacing value (Å) was obtained from a wide-angle X-ray diffraction (WAXD) pattern in the range of $5° \leq 2\theta \leq 50°$ using a Rigaku Denki Model RAD-C diffractometer (Tokyo, Japan). The X-ray generator was run at 40 kV and 100 mA.

The water vapor sorption data was obtained using a dynamic vapor sorption analyzer (DVS-1000, Surface Measurement System Ltd., London, UK) under 90% relative humidity (RH) at ambient temperature. The water uptake was determined by measuring the weight change of the membrane coupons after placement in liquid water at 30 °C for at least 1 day. The amount of free water in fully hydrated membranes was measured using a differential scanning calorimetry (DSC, DSC 2010 thermal analyzer, TA Instrument, DE, USA) [24]. For the measurement, DSC module was purged with nitrogen gas, quenched down to −50 °C with liquid nitrogen, and then heated up to +50 °C at a rate of 5 °C min^{-1}.

The proton conductivity (σ, S cm^{-1}) of each membrane coupon (size: 1 cm × 4 cm) was obtained using $\sigma = l/RS$ (l: distance between reference electrodes, and S: cross-sectional area of membrane coupon). Here, ohmic resistance (R) was measured by four-point probe alternating current (ac) impedance spectroscopy using an electrode system connected with an impedance/gain-phase analyzer (Solatron 1260) and an electrochemical interface (Solatron 1287, Farnborough Hampshire, ONR, UK) [26]. Impedance measurements were carried out in the thermo- and hygro-controlled chamber which was electrically shielded to avoid the influence of electromagnetic noise. The methanol permeability (P_{MeOH}, cm^2 s^{-1}) was measured at 30 °C using a two-chamber diffusion cell [24,25]. The glass diffusion cell consisted of two chambers (V = 60 mL) which were filled with 10 M (34 wt.%) methanol solution and deionized water, respectively. The methanol concentration was periodically measured using a gas chromatograph (Shimadtzu, GC-14B, Tokyo, Japan) equipped with a thermal conductivity detector (TCD).

Mechanical properties of the membranes were measured with an Instron mechanical testing machine (INSTRON-1708, Boston, MA, USA) following ASTM D882. Prior to determination of stability to hydrolysis, each membrane coupon was immersed in liquid water at 80 °C. Each measurement was repeated at least five times to guarantee good reproducibility of results.

2.5. Electrochemical single cell performances

The membrane-electrode assemblies (MEAs) based on each membrane in the present study were fabricated using catalyst coated membrane (CCM) method with a well-dispersed catalyst slurry. The catalyst slurry was sprayed on the membranes at ambient temperature. The resulting MEAs were dried at 60 °C in a vacuum oven. For PEMFC, 20 wt.% Pt/C (E-TEK, NJ, USA) was used to make a catalyst slurry and the Pt loading content on each electrode was 0.3 mg cm^{-2}. Meanwhile, Pt black and Pt–Ru black (Johnson Matthey Fuel Cells, PA, USA) were used for electrode fabrication with a constant loading content of 3 mg cm^{-2}.

3. Results and discussion

3.1. UAN as IPN-type crosslinker and dispersant

UAN is composed of a hydrophobic polypropylene oxide (PPO) segment and a hydrophilic polyethylene oxide (PEO) segment as illustrated in Fig. 1. Two kinds of reactive site exist at the terminal end of each segment in UAN. Within the polymer matrix, vinyl groups at the terminal end of the PPO segment are polymerized using AIBN as an initiator and form a IPN structure [17]. In addition, a hydroxyl (–OH) group at the terminal end of the PEO segment in UAN can react with functional groups in the polymer matrix and form peculiar microstructures combined with IPN and crosslinked structure. Here, pristine SPI was used as a polymer matrix having both sulfonic acid (–SO_3H) and carboxylic acid (–COOH) groups. In our previous studies, evidences in relation to crosslinking between –OH in crosslinkers and –COOH in the polymer matrix have been already presented [24,25].

Table 2
Solubility behavior of SPI membrane including IXSPI–SiO_2 in common polar aprotic solvents

Sample	NMP	DMAc	DMF	DMSO	*m*-Cresol
Pristine SPI–*d*	+	+	+	+	+
Pristine SPI–*m*	+	+	+	+	+
SPI–0–hl–1–*d*	+	+	+	+	+
SPI–0–hl–1–*m*	+	+	+	+	+
SPI–0–hb–1–*d*	+	+	+	+	+
SPI–0–hb–1–*m*	+	+	+	+	+
IXSPI–22–hl–0–*d*	–	–	–	–	–
IXSPI–22–hl–0–*m*	–	–	–	–	–
IXSPI–22–hl–1–*d*	–	–	–	–	–
IXSPI–22–hl–1–*m*	–	–	–	–	–
IXSPI–22–hb–1–*d*	–	–	–	–	–
IXSPI–22–hb–1–*m*	–	–	–	–	–
IXSPI–4–hl–1–*m*	–	–	–	–	–
IXSPI–13–hl–1–*m*	–	–	–	–	–
IXSPI–22–hl–1–*m*	–	–	–	–	–
IXSPI–74–hl–1–*m*	–	–	–	–	–

(+) Completely soluble; (–) completely insoluble in each solvent.

The solubility of each membrane in common organic solvents shown in Table 2 can be an important evidence to confirm the formation of a crosslinked structure. Generally, most SPI membranes were insoluble in polar aprotic solvents after imidization. The solubility of the SPI membranes can be improved by diamines with flexible groups such as ether (–O–) and thionyl (–S–), *m*-oriented diamines, and random sequence of diamine moieties [21,27–30]. To enhance processability of the resulting membrane, pristine SPI was designed and fabricated in a random copolyimide using SODA with a flexible ether group and *m*-substituted DBA. At elevated temperatures above 60 °C, pristine SPI was completely soluble in all organic solvent. However, IXSPI membranes containing a crosslinked polymer network were insoluble in the same solvents even at over 180 °C regardless of the presence of SiO_2.

UAN played a key role in the homogeneous distribution of nanosized SiO_2 as well as crosslinking with pristine SPI. Fig. 2(a) shows a FE-SEM image of IXSPI–22–hl–1. SiO_2 particles are not visible in the SEM image as compared with those of SPI–0–hl–1 or SPI–0–hb–1 containing SiO_2 particles without UAN. SiO_2 particles identified as bright dots were observed only in the Si-mapping image using the energy-dispersive spectrometer (EDS) attachment of FE-SEM. The TEM image of the composite membrane in Fig. 2(b) shows that SiO_2 particles were nanophase-separated within the pristine SPI matrix. The dark SiO_2 clusters were dispersed with an average size of 12–15 nm, which was similar to or slightly larger than the particle size of 12 nm used in the present study. This indicates that the incorporation of UAN–SiO_2 prevented aggregation or segregation of the inorganic particles and contributed to the formation of a con-

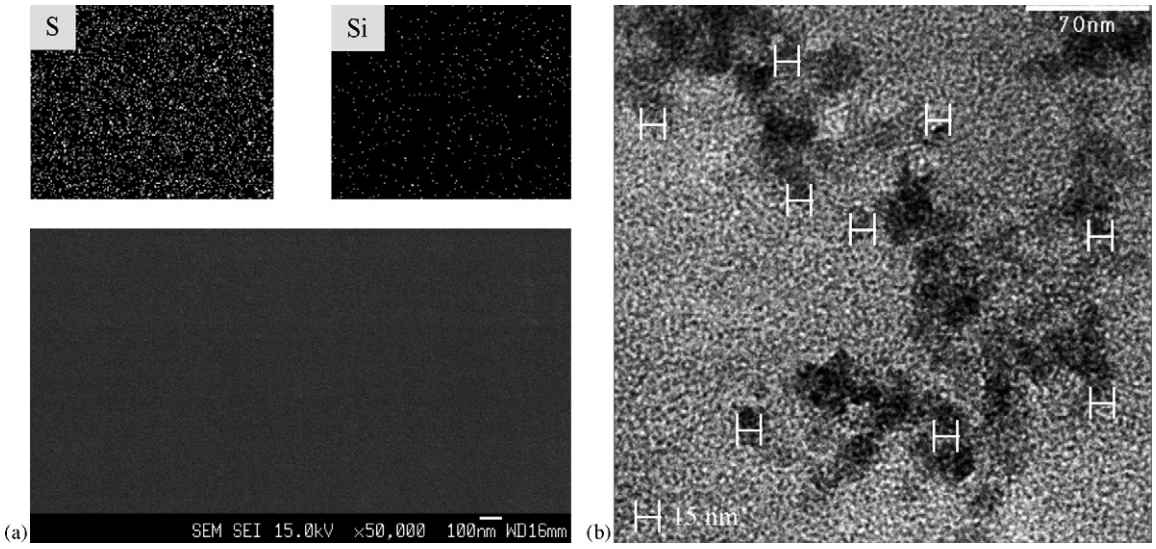

Fig. 2. (a) FE-SEM image accompanied by EDS images (1000×) and (b) TEM image of IXSPI–22–hl–1.

tinuous inorganic phase near the hydrophilic moieties of pristine SPI and UAN.

3.2. PEM performance of IXSPI–SiO_2 nanocomposite membranes

Water molecules absorbed in sulfonated polymer membranes lead to the formation of characteristic microstructures which results from negatively charged fixed ions (–SO_3H) [31,32]. The hydrated microstructure responsible for proton or methanol transport can be easily changed by structural modification [24,25] such as crosslinking and grafting or by the formation of composite membranes [17].

Furthermore, casting solvents also play an important role in the morphological change of membranes. Among NMP, DMAc, and DMF reported in the literatures [18–20], strong hydrogen bonding between DMF and –SO_3H in polymers prohibited spontaneous dissociation of protons and therefore reduced proton conductivity in an aqueous medium.

These changes in microstructure of the resulting polymers can be inferred by measuring both the amount of water and the state of water within the membranes. In particular, the state of water should be considered as an important factor to govern proton transport properties. The state of water is classified into three categories (free water, freezing bound water and non-freezing bound water) depending on the water's interaction with sulfonated polymers [31]. Here, non-freezing bound water has a strong interaction *via* ionic or hydrogen bonds with polar groups in the polymer matrices. The non-volatile bound water highly contributes to effective proton conduction.

Table 3
Hydrophilicity and *d*-spacing values of pristine SPI and IXSPI–SiO_2 nanocomposites fabricated using different casting solvents

Sample	Water vapor sorption at 90% RH (%)	Water uptake in liquid water (%)	Free water (%)	Bound water (%)	Bound water/total water × 100 (%)	*d*-Spacing (Å)	Activation energy (kJ (mol K)$^{-1}$)
Pristine SPI–*d*	28.5	33.8	16.3	17.5	51.8	4.19	6.39
Pristine SPI–*m*	28.8	34.2	16.1	18.1	52.9	4.21	6.39
SPI–0–hl–1–*d*	27.6	32.5	15.4	17.1	52.7	4.15	5.47
SPI–0–hl–1–*m*	28.5	33.7	15.4	18.3	54.3	4.17	5.27
SPI–0–hb–1–*d*	24.7	29.4	15.8	13.6	46.2	4.17	5.60
SPI–0–hb–1–*m*	25.3	29.8	15.9	13.9	46.5	4.18	5.44
IXSPI–22–hl–0–*d*	25.4	30.1	11.9	18.2	60.3	4.12	5.45
IXSPI–22–hl–0–*m*	25.7	30.4	11.9	18.5	60.8	4.15	5.39
IXSPI–22–hl–1–*d*	20.5	24.3	5.2	19.1	78.6	4.05	5.19
IXSPI–22–hl–1–*m*	21.3	25.0	5.3	19.7	78.8	4.07	4.98
IXSPI–22–hb–1–*d*	18.8	22.5	10.1	12.4	55.2	4.09	5.21
IXSPI–22–hb–1–*m*	19.2	22.7	10.1	12.6	55.6	4.12	5.25
IXSPI–4–hl–1–*m*	20.1	23.7	6.8	16.9	71.4	3.92	5.41
IXSPI–13–hl–1–*m*	20.7	24.6	6.6	18.0	73.2	3.96	4.91
IXSPI–22–hl–1–*m*	21.3	25.0	5.3	19.7	78.8	4.07	4.98
IXSPI–74–hl–1–*m*	23.9	28.3	5	23.3	82.2	4.16	5.05

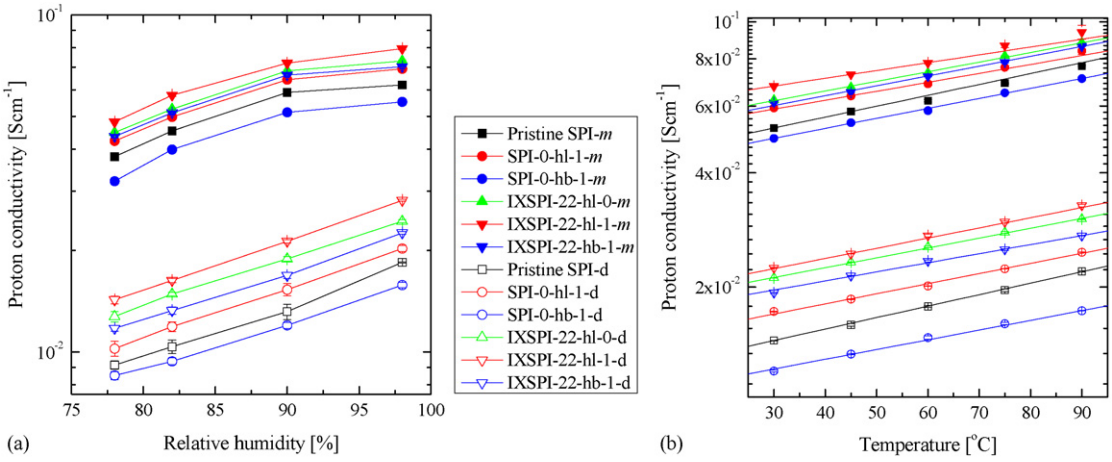

Fig. 3. Proton conductivity of SPI membranes (a) as a function of humidity at 60 °C and (b) as a function of temperature at 95% RH.

Table 3 shows the water uptake properties of SPI membranes derived from different kinds of SiO_2 nanoparticles and casting solvents. UAN containing hydrophilic PEO segments increased bound water content in IXSPI–22–hl–0 compared with that in pristine SPI. The addition of hydrophilic SiO_2 (SPI–0–hl–1) also resulted in a small increase of bound water content owing to –OH groups on the surface of SiO_2. On the other hand, hydrophobic SiO_2 reduced bound water content in the resulting composite (SPI–0–hb–1). This trend is clearly observed even in the integrated systems of SiO_2 accompanied by UAN (IXSPI–22–hl–1 and IXSPI–22–hb–1), indicating an important role of hydrophilic SiO_2.

This characteristic state of water in the membranes affected their proton conduction behavior as shown in Fig. 3. Proton conductivity of pristine SPI was improved after incorporation of UAN and hydrophilic SiO_2. IXSPI–22–hl–1 showed the highest proton conductivity *via* a synergetic effect of UAN and hydrophilic SiO_2. In contrast, hydrophobic SiO_2 suppressed an enhancement of bound water by PEO segments in UAN and reduced the proton conductivity of IXSPI–22–hb–1 to a level lower than that of IXSPI–22–hl–0.

We noticed that the choice of casting solvent markedly influenced the properties of resulting membranes, particularly bound water and proton conductivity. Note that all the SPI membranes fabricated using DMSO as a casting solvent exhibited low bound water content in comparison with those using *m*-cresol as shown in Table 3. Interestingly, the use of DMSO and *m*-cresol as casting solvents also led to significantly different proton transport behavior in the resulting SPI membranes, regardless of surface properties of SiO_2. The strong interaction between sulfonic acid groups in the polymer matrix and DMSO molecules as illustrated in Fig. 4 reduced the proton conductivity of the resulting membranes to a very low level along with a decrease in their bound water content. This implies that DMSO is a poor casting solvent for PEM fabrication.

In DMFC application, methanol transport behavior across sulfonated polymer membranes is highly dependent on their total water uptake values shown in Table 3 [23,24,32,33]. This is because protons form ionic complexes (H_3O^+ and $CH_3OH_2^+$) with water and methanol, and transport in the complex form from anode to cathode through peculiar hydrated microstructures in the membranes. Therefore, it is desirable to achieve a high barrier property of the membranes to methanol molecules by controlling water uptake.

Fig. 5 shows the methanol permeability and selectivity of SPI membranes. Here, a characteristic factor, selectivity ($\Phi =$

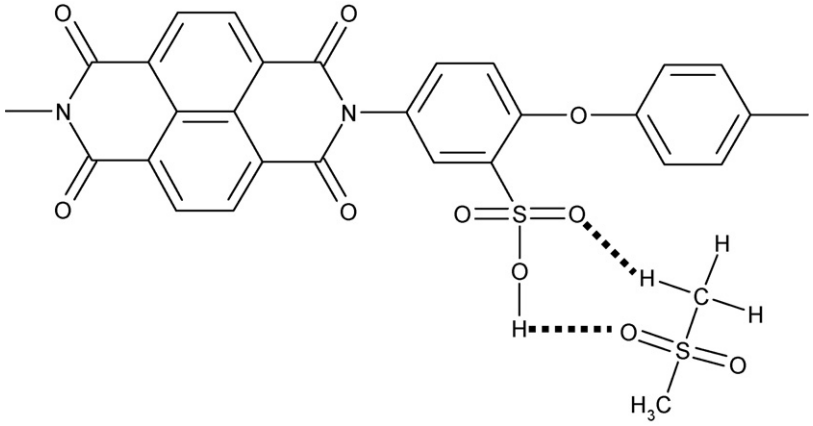

Fig. 4. Physico-chemical interaction of DMSO with sulfonic acid group in SPI matrix through secondary hydrogen bond.

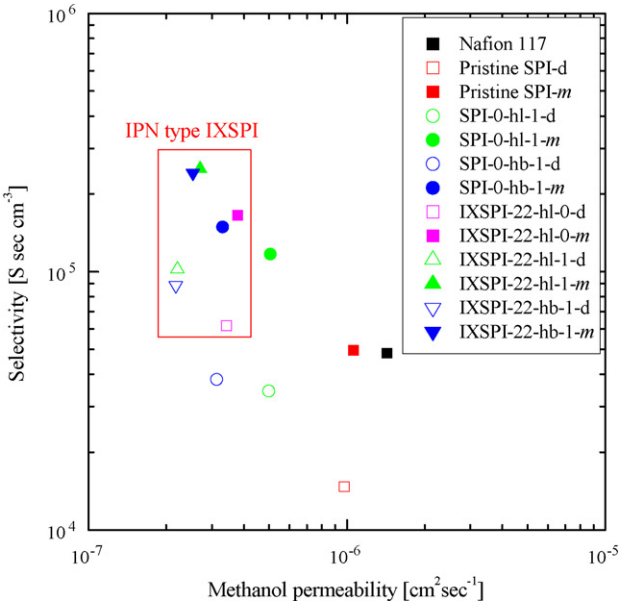

Fig. 5. Methanol permeability and selectivity of Nafion 117 and SPI membranes at 30 °C.

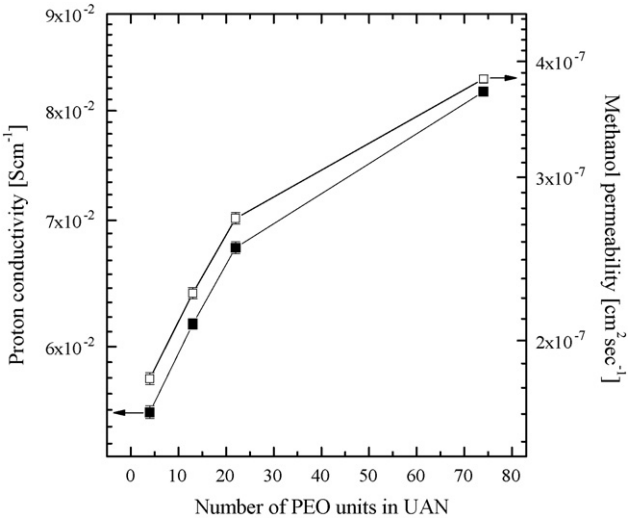

Fig. 6. Influence of crosslinker size on membrane performances. Proton conductivity and methanol permeability were measured at 30 °C and 95% RH, and 30 °C using 10 M methanol solution, respectively.

σP_{MeOH}^{-1}) is generally used to evaluate both proton conductivity and methanol permeability. The water uptake level of pristine SPI membranes which is similar to that (35.2%, measured) of Nafion 117, induced high methanol permeabilities of 10^{-6} cm^2 s^{-1}. However, SiO_2 nanoparticles reduced vacancies (so called water pockets) where the absorbed water molecules could remain, and decreased water uptake of resulting composites. Consequently, SiO_2 particles obstructed methanol permeation through the composite membranes to some extent and improved their selectivity. This effect was more apparent in SPI–0–hb–1 than in SPI–0–hl–1. In IXSPI–22–hl–0, crosslinking based on UAN also gave rise to a reduction of water uptake and, thereby, led to lower methanol permeability and higher selectivity than those of pristine SPI. The integration of SiO_2 using UAN resulted in a considerable reduction of water uptake and an improved methanol-barrier property. Unlike the composites (SPI–0–hl–1 or SPI–0–hb–1) containing only SiO_2 particles, the effect of SiO_2 in relation to the reduction of methanol permeability was not remarkable in IXSPI–SiO_2 nanocomposite membranes where the methanol transport properties were similar irrespective of the type of SiO_2. Consequently, IXSPI–22–hl–1 with proton conductivity enhanced by hydrophilic SiO_2 showed higher selectivity than IXSPI–22–hb–1.

In addition to the effects of UAN and SiO_2, casting solvents also affected membrane performances including selectivity. The solvent effect on methanol permeability was minimal, but large differences in proton conductivity caused SPI membranes fabricated using DMSO to have lower selectivities than those using *m*-cresol. In summary, the usage of hydrophilic SiO_2 and *m*-cresol was desirable to fabricate IXSPI composite membranes with high performances.

It is essential to select a crosslinker with an appropriate chain length when considering membrane performances in crosslinked SPI systems [25]. To examine the effects of the size of the crosslinker, hydrophilic fumed SiO_2 and *m*-cresol were used as the nanosized SiO_2 particle and casting solvent, respectively, for membrane fabrication. The crosslinker size in the IXSPI system was controlled by changing only the length of the hydrophilic PEO segments in UAN.

Fig. 6 exhibit a correlation between the length of PEO segments in the IPN-type crosslinker and PEM performances. As shown in Table 3, the increase in the number of PEO units from 4 to 74 widened the average interchain distance between SPI chains and induced high water uptake in the resulting IXSPI–SiO_2 nanocomposites. Accordingly, their methanol permeability increased successively from 1.82×10^{-7} to 3.83×10^{-7} cm^2 s^{-1} at 30 °C. Simultaneously, longer crosslinker reinforced interaction of PEO segment with water molecules and raised bound water content resulting in improved proton conductivity. However, the increase in methanol permeability was greater than the increase of proton conductivity, which reduced the selectivity from 3.04×10^5 S s cm^{-3} (IXSPI–4–hl–1–*m*) to 2.14×10^5 S s cm^{-3} (IXSPI–74–hl–1–*m*).

3.3. Physico-chemical properties of IXSPI–SiO_2 nanocomposite membranes

The mechanical strength of sulfonated polymer membranes is another important factor to consider for the MEA fabrication process. If sulfonated polymer membranes with excellent PEM performances have low mechanical properties, the membranes are useless because membrane breakage can easily occur during the MEA formation process. In other words, membrane materials with high mechanical strength are required to obtain MEAs with high electrochemical performances. The addition of SiO_2 nanoparticles presented in Table 4 enhanced the mechanical properties of the resulting SPI membranes to some extent, irrespective of the type of SiO_2. In the case of the IXSPI membranes, the tensile strength increased more than 6%, and the elongation almost tripled owing to an extensible IPN structure containing

Table 4
Physico-chemical properties including hydrolytic stability of SPI membranes

Sample	Elongation (%)	Hydrolytic stability (days)[a]	Proton conductivity (10^2 S cm^{-1})		Tensile strength (MPa)	
			Before	After	Before	After
Pristine SPI–*d*	2.3	2.8	1.44	1.38	93.8	92.1
Pristine SPI–*m*	2.5	2.9	5.25	5.01	96.0	94.4
SPI–0–hl–1–*d*	3.8	214.6	1.72	1.64	95.0	93.2
SPI–0–hl–1–*m*	3.9	233.3	5.93	5.68	99.2	97.5
SPI–0–hb–1–*d*	3.7	237.5	1.20	1.19	97.5	95.8
SPI–0–hb–1–*m*	3.8	250.0	4.93	4.73	97.6	95.8
IXSPI–22–hl–0–*d*	7.5	116.7	2.11	2.02	99.3	97.7
IXSPI–22–hl–0–*m*	7.3	133.3	6.23	5.94	100.4	99.1
IXSPI–22–hl–1–*d*	8.1	>291.7[b]	2.25	2.17	99.9	97.7
IXSPI–22–hl–1–*m*	7.7	>291.7[b]	6.77	6.46	102.3	100.7
IXSPI–22–hb–1–*d*	7.9	>291.7[b]	1.93	1.86	99.4	97.6
IXSPI–22–hb–1–*m*	7.3	>291.7[b]	6.13	5.84	101.4	99.8
IXSPI–4–hl–1–*m*	8.2	>291.7[b]	5.54	5.30	101.9	100.4
IXSPI–13–hl–1–*m*	7.9	>291.7[b]	6.17	5.88	103.2	101.6
IXSPI–22–hl–1–*m*	7.7	>291.7[b]	6.77	6.46	102.3	100.7
IXSPI–74–hl–1–*m*	7.9	>291.7[b]	8.19	7.82	100.3	98.7

[a] The elapsed time that proton conductivity and tensile strength did not change within ±5% and ±2%, respectively.
[b] The hydrolytic stabilities of the SPI membranes are still being measured using changes of proton conductivity and tensile strength.

flexible urethane (–NH–C=O–O–) groups. The improvement of mechanical properties was prominently observed in IXSPI–SiO_2 nanocomposite membranes containing both SiO_2 and UAN. This might result from a homogeneous dispersion of nanosized SiO_2 as well as high extension of IPN based on UAN.

Together with mechanical properties, a high resistance to hydrolytic degradation is also indispensable to accomplish excellent single cell performances of MEAs based on sulfonated polymer membranes. In particular, low water stability of SPI membranes in the hydrated medium has been recognized as a severe obstacle to prevent the development of PEM based on SPI. Until, relevant studies have been carried out with an objective to improve the durability to hydrolysis of SPI membranes in acidic liquid water. The researches have included the use of hydrolytically durable monomers [22,27,28,32,34–37] and crosslinkers [24,25,32,35–37]. The hydrolytic stabilities of the resulting SPI membranes are still not satisfactory for long-term fuel cell operation.

In the present study, the hydrolytic stabilities of SPI membranes were evaluated by measuring changes in proton conductivity [24,25,32] and mechanical strength [35–38] after immersion in hot water at 80 °C. Despite that the fact that pristine SPI contains a naphthalenic polyimide structure with higher durability than a phthalic polyimide structure [34], its proton conductivity and mechanical properties were easily changed within 3 days. However, the rapid hydrolytic decomposition of pristine SPI was deactivated after successive incorporation of UAN and SiO_2. Surprisingly, the resistance to hydrolytic attack of IXSPI–SiO_2 nanocomposites increased by a factor of about 100. The unexpected results may be related to an improvement of chemical stability in the poly(ethylene glycol) (PEG)–SiO_2 nanocomposite [5,39]. That is, nanosized fumed SiO_2 may deactivate the hydrolytic decomposition in acidic water medium by trapping water molecules (hydrophilic SiO_2) or repelling water molecules (hydrophobic SiO_2). In addition to SiO_2 effect, an increase of molecular weight of pristine SPI after crosslinking may slow down the hydrolysis reaction rate of SPI chains. Also, the water stability of UAN–SiO_2 was more apparent in IXSPI–SiO_2 nanocomposites fabricated using *m*-cresol than those using DMSO.

3.4. Single fuel cell performances of MEAs based on IXSPI–SiO_2 nanocomposite membranes

Fig. 7 exhibits electrochemical single cell results based on IXSPI membranes at 80 °C. Nafion 117 and pristine SPI–*m* were used as control materials. In PEMFC application in Fig. 7(a), a crosslinker with a long PEO segment strongly contributed to improvement of electrochemical properties in the resulting IXSPI–SiO_2 nanocomposite membranes owing to a high dependence of proton conductivity on crosslinker size. IXSPI–74–hl–1–*m* containing the longest PEO chains showed an outstanding single cell performance (800 mA cm^{-2} at 0.6 V and maximum power density = 598.4 mW cm^{-2} at 0.44 mA cm^{-2}) superior to Nafion 117 (720 mA cm^{-2} at 0.6 V and maximum power density = 583.4 mW cm^{-2} at 0.43 mA cm^{-2}). Even in IXSPI–22–hl–1 with the same crosslinker size and SiO_2 content, the use of DMSO as casting solvent gave rise to a large decrease in the proton conductivity, resulting in undesirable single cell performance in comparison with the nanocomposite membrane fabricated using *m*-cresol.

The same trend was also observed in Fig. 7(b) indicating the predominant influence of proton conductivity on single cell performances even in DMFC using methanol as fuel. In spite of higher methanol permeability, the electrochemical properties of IXSPI–SiO_2 nanocomposite membranes increased as the chain

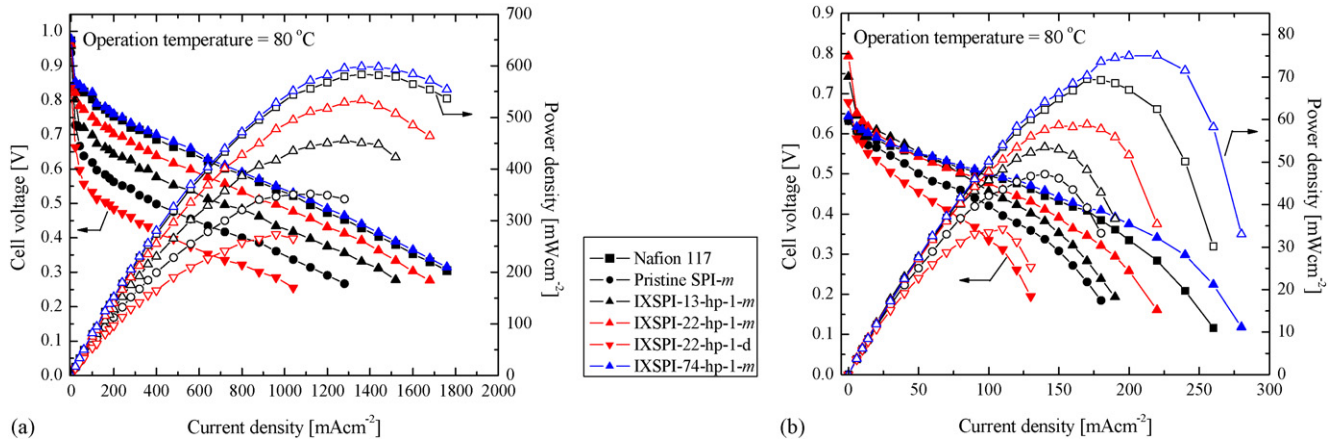

Fig. 7. Single cell performances of Nafion 117, pristine SPI–*m*, IXSPI–13–hl–1–*m*, IXSPI–22–hl–1–*m*, and IXSPI–74–hl–*m* under (a) PEMFC (H_2/O_2 = 200 cm^3 min^{-1}/200 cm^3 min^{-1}) and (b) DMFC (1 M MeOH/O_2 = 1 cm^3 min^{-1}/200 cm^3 min^{-1}) operation condition.

length of PEO units in IPN-type crosslinkers was longer and their proton conductivities were enhanced. The high methanol permeability (1.43×10^{-6} cm^2 s^{-1}) of Nafion 117 made a difference in the single cell results with IXSPI–74–hl–1–*m* causing the performances in DMFC to be larger than those in PEMFC. At present, our on-going studies focus on the long-term operation of MEAs based on the IXSPI–SiO_2 system under fuel cell operating conditions and this work will be reported shortly.

4. Conclusions

The following conclusions can be drawn from the present study:

(1) Crosslinked IXSPI–SiO_2 nanocomposite membranes containing IPN structure were successfully fabricated through a consecutive two-step synthetic route of (1) preparation of pristine SPI and (2) direct mixing of UAN and nano-sized fumed SiO_2. Here, UAN played important roles in the homogeneous distribution of SiO_2 nanoparticles and, simultaneously, crosslinking with pristine SPI accompanied by an IPN structure.

(2) The addition of UAN increased bound water content and then improved proton conductivity in the resulting membrane. Crosslinking based on an IPN-type crosslinker reduced the water uptake level and led to an enhancement of methanol-barrier property and membrane durability. Urethane groups in UAN significantly contributed to the formation of an extensible IPN structure. Surprisingly, the water stability of the resulting nanocomposites increased to about 10 months.

(3) The casting solvent affected PEM performances of resulting SPI membranes such as hydrophilicity, proton conductivity, methanol permeability, mechanical strength, and hydrolytic stability. Regardless of the type of SiO_2, a strong interaction of DMSO with $-SO_3H$ groups in pristine SPI matrix reduced the number of protons responsible for charge transfer, inducing a dramatic drop in proton conductivity. In spite of the lower water uptake level and methanol permeability, the single cell performances based on the nanocomposite membrane derived from DMSO was much lower than those from *m*-cresol even in DMFC owing to the high dependence of cell performance on proton conductivity. The use of DMSO as a casting solvent was incongruent for the fabrication of PEM with excellent physicochemical and electrochemical properties.

(4) The PEO chain length of IPN-type crosslinker affected membrane performances in the resulting IXSPI–SiO_2 nanocomposite membranes. Incorporation of long crosslinker increased proton conductivity and methanol permeability. The single cell performances of IXSPI–SiO_2 nanocomposite with longer PEO chains were more improved than those with shorter PEO chains in both PEMFC and DMFC.

Acknowledgements

The authors would like to thank the Ministry of Commerce, Industry, and Energy for funding this research (Grant M1042503000704L250300710). C.H. Lee, S.Y. Hwang, and J.Y. Sohn are very grateful to the BK21 Project for a fellowship.

References

[1] Z. Chen, L.A. Samuelson, J. Akkara, D.L. Kaplan, H. Gao, J. Kumar, K.A. Marx, S.K. Tripathy, Chem. Mater. 7 (1995) 1779.
[2] M. Yoshita, P.N. Prasad, Chem. Mater. 8 (1996) 235.
[3] H.W. Oviatt Jr., K.J. Shea, S. Kalluri, Y. Shi, W.H. Steier, L.R. Dalton, Chem. Mater. 7 (1995) 493.
[4] S.D. Balla, I. Fragala, M.A. Ratner, T.J. Marks, Chem. Mater. 7 (1995) 400.
[5] S.R. Raghavan, M.W. Riley, R.S. Fedkiw, S.A. Khan, Chem. Mater. 10 (1998) 244.
[6] K. Kanamura, T. Mitsui, H. Munakata, Chem. Mater. 17 (2005) 4845.
[7] P.L. Antonucci, A.S. Arico, P. Creti, E. Ramunni, V. Antonucci, Solid State Ionics 125 (1999) 431.
[8] Z. Shao, P. Joghee, I. Hsing, J. Membr. Sci. 229 (2004) 43.
[9] A.S. Aricò, V. Baglio, A.Di. Blasi, E. Modica, P.L. Antonucci, V. Antonucci, J. Power Sources 128 (2004) 113.

[10] A. Saccà, I. Gatto, A. Carbone, R. Pedicini, E. Passalacqua, J. Power Sources. 163 (2006) 47–51.
[11] D.S. Kim, H.B. Park, J.W. Rhim, Y.M. Lee, J. Membr. Sci. 240 (2004) 37.
[12] D.S. Kim, H.B. Park, J.W. Rhim, Y.M. Lee, Solid State Ionics 176 (2005) 117.
[13] H.B. Park, Y.M. Lee, Adv. Mater. 17 (4) (2005) 477.
[14] R.K. Nagarale, G.S. Gohil, V.K. Shahi, R. Rangarajan, Macromolecules 37 (2004) 10023.
[15] D.H. Jung, S.Y. Cho, D.H. Peck, D.R. Shin, J.S. Kim, J. Power Sources 106 (2002) 173.
[16] P. Staiti, A.S. Arico, V. Baglio, F. Lufrano, E. Passalacqua, V. Antonucci, Solid State Ionics 145 (2001) 101.
[17] J.Y. Kim, S. Mulmi, C.H. Lee, H.B. Park, Y.M. Lee, J. Membr. Sci. 283 (2006) 172.
[18] G.P. Roberson, S.D. Mikhailenko, K. Wang, P.X. Xing, M.D. Guiver, S. Kaliaguine, J. Membr. Sci. 219 (2003) 113.
[19] J. Kim, B. Kim, B. Jung, Y.S. Kang, H.Y. Ha, I.H. Oh, K.J. Ihn, Macromol. Rapid Commun. 23 (2002) 753.
[20] R. Guan, H. Dai, C. Li, J. Liu, J. Xu, J. Membr. Sci. 277 (2005) 148.
[21] F. Vidal, O. Fichet, J. Laskar, D. Teyssié, Polymer 47 (2006) 3747.
[22] J. Fang, X. Guo, S. Harada, T. Wateri, K. Tanaka, H. Kita, K. Okamoto, Macromolecules 35 (2002) 9022.
[23] J.Y. Kim, D.H. Shin, K.J. Ihn, C.W. Nam, Macromol. Chem. Phys. 203 (2002) 2454.
[24] C.H. Lee, H.B. Park, Y.S. Chung, Y.M. Lee, B.D. Freeman, Macromolecules 39 (2006) 755.
[25] H.B. Park, C.H. Lee, Y.M. Lee, B.D. Freeman, H.J. Kim, J. Membr. Sci. 285 (2006) 432–443.
[26] C.H. Lee, H.B. Park, Y.M. Lee, R.D. Lee, Ind. Eng. Chem. Res. 44 (2005) 7617.
[27] C. Genies, R. Mercier, B. Sillion, N. Cornet, G. Gebel, M. Pineri, Polymer 42 (2001) 359.
[28] X. Guo, J. Fang, T. Wateri, K. Tanaka, H. Kita, K. Okamoto, Macromolecules 35 (2002) 6707.
[29] T. Wateri, J. Fang, K. Tanaka, H. Kita, K. Okamoto, T. Hirano, J. Membr. Sci. 230 (2004) 111.
[30] Z. Hu, Y. Yin, S. Chen, O. Yamada, K. Tanaka, H. Kita, K. Okamoto, J. Polym. Sci. Part A: Polym. Chem. 44 (2006) 2862.
[31] K.D. Kreuer, J. Membr. Sci. 185 (2001) 29.
[32] Y.M. Lee, Macromolecular Engineering: From Precise Macromolecular Synthesis to Macroscopic Materials Properties and Application, Membranes and Fuel Cell, Proton Exchange Membrane for Fuel Cell Systems: Structure–Property Relationships, Wiley–VCH, 2006.
[33] L.E. Karlsson, B. Wesslen, P. Jannasch, Electrochim. Acta 47 (2002) 3269.
[34] C. Genies, R. Mercier, B. Sillion, R. Petiaud, N. Cornet, G. Gebel, M. Pineri, Polymer 42 (2001) 5097.
[35] Y. Yin, O. Yamada, K. Tanaka, K. Okamoto, Polym. J. 38 (3) (2006) 197.
[36] Y. Yin, Y. Suto, T. Sakabe, S. Chen, S. Hayashi, T. Mishima, O. Yamada, K. Tanaka, H. Kita, K. Okamoto, Macromolecules 39 (2006) 1189.
[37] Y. Yin, O. Yamada, S. Hayashi, K. Tanaka, H. Kita, K. Okamoto, J. Polym. Sci. Part A: Polym. Chem. 44 (12) (2006) 3751.
[38] C.D. Rio, J.R. Jurado, J.L. Acosta, Polymer 46 (2005) 3975.
[39] Y. Fu, X. Ma, Q. Yang, X. Zong, Mater. Lett. 57 (2003) 1759.